CSCE 2021 Annual Conference
Inspired by Nature – Inspiré par la Nature

26-29 May 2021

TENSILE PROPERTIES OF PET FRP WITH BIO-RESIN POLYMER

Kassab, R[1, 2], and Sadeghian, P[1]
[1] Dalhousie University, Canada
[2] R.Kassab@dal.ca

Abstract: This study analyses the mechanical behaviour of polyethylene terephthalate fiber-reinforced polymer (PET FRP) made with a bio-resin polymer matrix. The utilized bio-resin is furfuryl alcohol mixed with phthaloyl dichloride catalyst; this selection of resin type, catalyst type, catalyst dose, and curing time was made based on previous investigations. A sheet of PET FRP composite was fabricated following the wet lay-up method. The composite sheet was cut into six coupons (three in the longitudinal direction and three in the transverse direction). The coupons were then tested in uniaxial tension, and the stress-strain relationship was extracted. The stress-strain relationship of the bio-resin PET FRP was found to be nonlinear and consisted of three main stages of linear curves. The elastic modulus at each stage was derived along with the coupon's average yielding stress and ultimate strength. By deriving and presenting the mechanical performance of this newly developed FRP, this study aims to determine whether the composite could be a potentially sustainable alternative to conventionally used FRPs. The two sets of tested coupons had equal strain capacity–which is four times the strain capacity of glass fiber-reinforced (GFRP) composite. Conversely, longitudinally cut coupons had double the strength capacity of transversely cut coupons.

1 INTRODUCTION

Today's fiber-reinforced polymers (FRPs) are composed of petroleum-based polymers and various types of fiber (Foruzanmehr et al. 2016). The type of fiber used significantly affects the overall composite strength, while the polymer component translates the load and maintains the fibers' orientation (Uddin et al. 2013). When considering a cradle-to-gate life cycle assessment (LCA), conventionally used FRPs composites may not be the proper choice for a sustainable material; the production process of conventionally used FRPs consumes a vast amount of energy, raw material, and water. Concurrently, through the various stages within their production process, pollutants outflow to the air, water, and land (Lee et al. 2020). To reduce the environmental impact of commonly used FRPs, recent studies have explored the use of different fiber and polymer types, namely natural fibers (Betts et al. 2017; Ghalieh et al. 2017) and bio-resin (Bachmann et al. 2017), respectively.

This study proposes a new type of FRP made from bio-resin polymer and polyethylene terephthalate (PET) fibers. Replacing traditionally used petroleum-based polymers (e.g., epoxy, polyester, vinyl ester) with bio-sourced resin reduces the composite's carbon footprint (Loong et al. 2018). The bio-resin and hardener used in this study—furfuryl alcohol and phthaloyl dichloride—was supplied by Pennakem under the trade name QuaCorr 1001 and QuaCorr 2001, respectively. Furfuryl alcohol is distinguished by thermosetting properties, physical strength, and corrosion resistance; thus, primarily used as a resin (Mamman et al. 2008). A study conducted by Fam et al. analyzed the mechanical performance of glass fiber-reinforced (GFRP) composite made from furfuryl alcohol resin and concluded that GFRP coupons made with said

resin mixed with 3% (by weight) phthaloyl dichloride reached the same tensile strength as GFRP coupons made with epoxy polymer (Fam et al. 2014). Consequently, this study used the same ratio of bio-resin to hardener. The continuous PET fibers were provided by Carthage Mills in the form of bi-directional fabric. Currently, this fabric is primarily used as a high-strength geotextile liner (Applications of Geosynthetic Products, 2020).

2 TESTING PROGRAM

The testing program objective is to analyze the behaviour of bio-resin PET FRP composite in tension. Coupons were created and tested in uniaxial tension based on standards from the American Society for Testing and Materials (ASTM 2018), which relates to composite thermoplastic material testing. Conclusions determined the ultimate tensile strength and strain attained by those coupons and stress-strain diagrams, illustrating a continuous representation of the stress-strain behaviour as coupons reach their ultimate tensile strength value. Moreover, based on the data obtained through the tension test, the elastic modulus is estimated following the calculation procedure outlined in the ASTM.

2.1 Fabrication of PET Coupons

Fabric made of woven PET fibers was combined with two-part bio-resin (QuaCorr 1001 and QuaCorr 2001) in a wet lay-up process to create the PET FRP composite sheet. Figure 1 shows the fabrication process of the PET FRP composites. The sheet was composed of two PET fabric layers—shown in Figure 1 (a)—with three layers of resin spread evenly between the fabric's surfaces, as shown in Figure 1 (b) and (d). Each dry fabric layer was approximately 1mm thick. The composite sheet was left to cure for 13 days at room temperature.

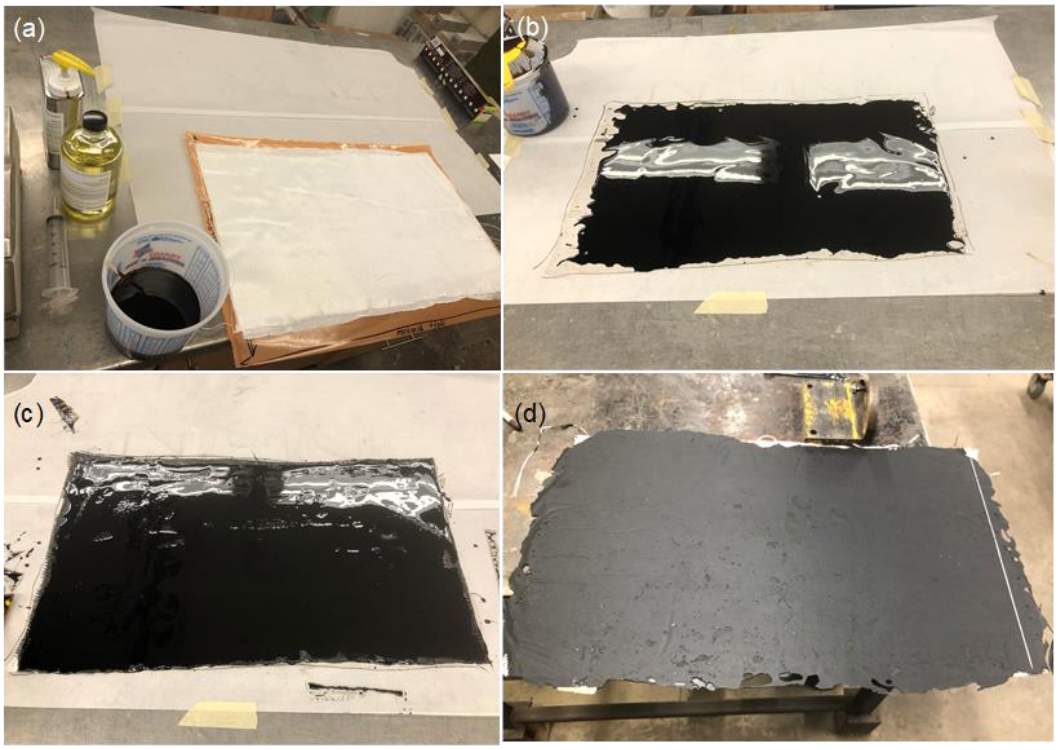

Figure 1: Fabrication of PET FRP composite sheet: (a) woven PET fabric prepared for the wet lay-up procedure; (b) first layer of bio-resin spread on parchment paper; (c) the second layer of bio-resin spread on PET fabric; and (d) cured PET FRP composite sheet.

The composite sheet was always covered with weights during the curing stage, allowing excess epoxy to outflow from the sides. The overall thickness of the composite was approximately 2mm, which varied among coupons. Figure 1 (d) illustrates the composite sheet following the curing period. Six PET FRP coupons were cut from the composite sheet—three coupons longitudinally and three transversely—presenting identical dimensions: 250mm length and 25mm width. The longitudinal direction is described as the direction parallel to weft fibres' orientation, whereas the transverse direction is parallel to warp fibres' orientation.

2.2 Instrumentation and Testing Procedure

All fabricated coupons were tested under the same conditions in uniaxial tension. Prior to testing, each coupon's width and thickness were measured using a digital calliper at three different locations: two near the coupons' ends and one mid-length. Due to the wet lay-up process used in fabrication, the six coupons' cross-sectional area differed slightly. An Instron 8501 (material testing machine) was used for the uniaxial tension test. Following ASTM D882 standard (ASTM 2018), 50mm of the coupon's length was placed within the Instron's grips from each end. Hence, 150mm of the coupon's length was laterally unsupported. The Instron's jaws then firmly gripped the ends of the FRP coupons. Furthermore, the jaws were carefully aligned to avoid coupon twisting during testing, which could generate poor data procurement or premature failure.

Since PET fibers hold large strain capacity, an extensometer was used instead of a conventional strain gauge to measure the strain change. Before initiating the tension test, the loading rate (displacement-controlled) was set to 2mm per minute, and a strain extensometer was clipped to coupon at mid-length. The extensometer and the Instron's load cell were attached to the data acquisition unit (DAQ). The DAQ was set to record the change in strain and load at an interval of 0.1 seconds. Figure 2 (a) reveals one of the PET FRP coupons firmly gripped by the Instron's jaws, with an extensometer fixed mid-length prior to applying the load. The test data was processed by the DAQ until the coupon reached its ultimate capacity and consequently failed in tension. The test was then terminated. Figure 2 (b) illustrates a coupon after reaching its ultimate tensile capacity.

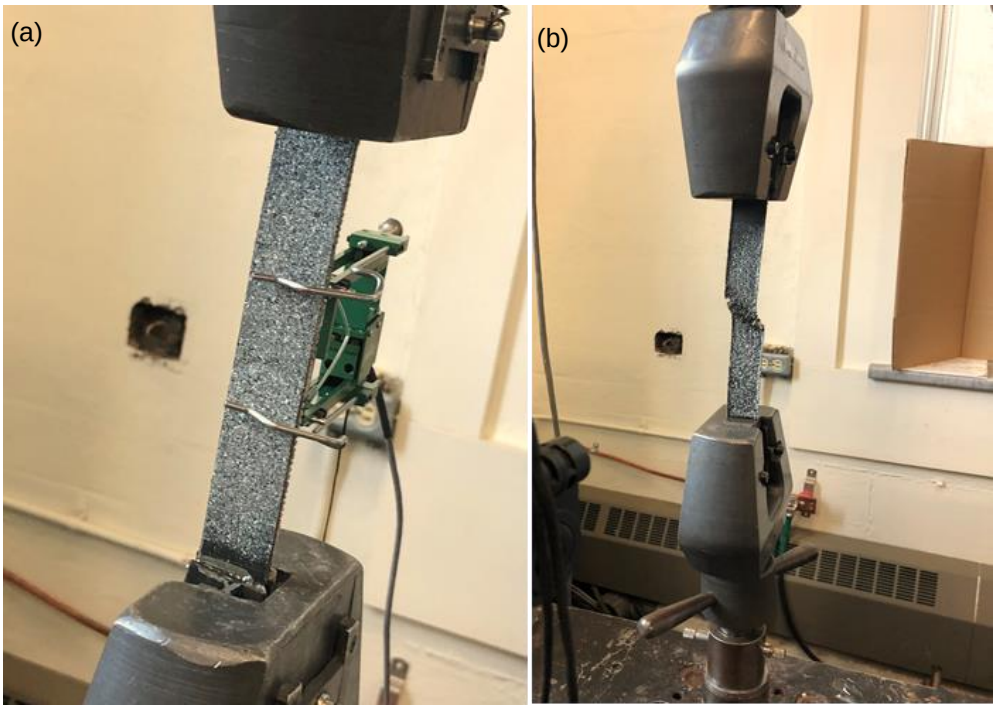

Figure 2: PET FRP coupons fixed on the Instron testing machine: (a) intact specimen before testing and (b) after the test was terminated and specimen reached its ultimate strength.

As shown in Figure 2 (b), failure developed diagonally along with the coupon at mid-length. This mode of failure persistently occurred with all tested coupons. After test completion, strain and load-resistance changes were outputted from the DAQ and converted into stress-strain data. Stress was calculated by dividing the load applied by the average cross-sectional area of individual coupons. All load steps were then converted to stress, and the ultimate strength of all coupons was found accordingly.

3 DATA ANALYSIS AND TEST RESULTS

The three PET FRP coupons from each set (longitudinal and transverse) concluded relatively similar testing results regarding strain deformation and strength capacity. Therefore, based on ASTM D882 standards, there was no requirement to test and create more coupons. Figure 3 illustrates the tested coupons after reaching their ultimate strength. As shown, failure occurred at the mid-length location; thus, there was no visual evidence of premature failure. Furthermore, longitudinal coupons provided a larger strength capacity compared to transverse coupons.

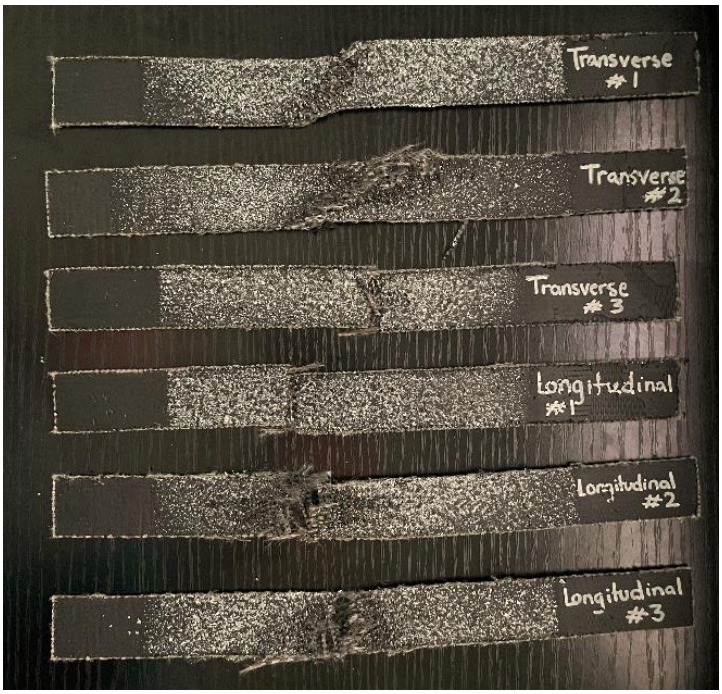

Figure 3: PET FRP coupons after reaching their ultimate tensile strength capacity.

The ultimate tensile strength of longitudinal coupons was found to be between 112 MPa and 120 MPa with a standard deviation of 5 MPa and coefficient of variation of 11%. Among the three specimens, the ultimate tensile strength of transverse coupons varied between 55 MPa and 71 MPa MPa with a standard deviation of 8 MPa and coefficient of variation of 13%. Therefore, the ratio of longitudinal to transverse fiber density is 2:1. The ultimate strain capacity was found to be approximately 10% for both longitudinal and transverse coupons. Hence, PET FRP has approximately five and six times more strain capacity compared to conventionally used unidirectional glass FRP (GFRP) and carbon FRP (CFRP) composites, respectively (Pham et al. 2015).

Figure 4 (a) corresponds to the stress-strain relationship of longitudinal coupons and (b) to transverse coupons. The nonlinear stress-strain curve of PET FRP is broken down into three regions; each region corresponds to a linear behaviour and features a unique modulus. The modulus at each region corresponds

to the slope of its linear stress-strain plot. As demonstrated in Figure 4, the PET FRP stress-strain relationship initially follows a linear trend. The modulus at this region (region 1), E_1, is the highest through the plot. After the coupon reaches the yielding stress, F_y, the modulus—E_2—significantly decreases. The average yielding stress of the longitudinal and transverse coupons was approximately 30 ± 6 MPa and 19 ± 1 MPa, respectively. At region 2, the coupon will undergo plastic deformation. Following this stage, the modulus will change one final time. At region 3, the modulus (E_3) increases but is still lower than the initial modulus. Region 3 corresponds to a strain hardening behaviour that result after the specimen stretches beyond its natural stretch ratio (NSR). Hence, the transition point between region 2 and region 3 is referred to as "hardening point" with a distinct hardening stress, F_h, and strain, ε_h.

Using the plots presented in Figure 4, three moduli were calculated for each PET FRP types. The juncture between the first two linear curves is assumed as a yielding point. Hence, the yielding stress and strain were extracted from the plot using the 0.2% offset method. The key properties of the tested coupons, extracted from the plots presented in Figure 4, are listed in Table 1 and Table 2.

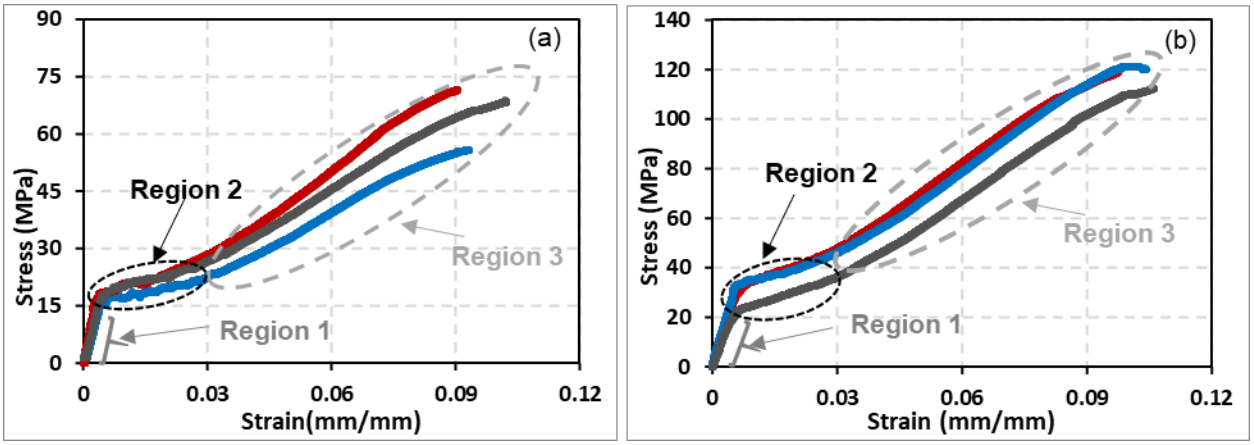

Figure 3: Stress-strain plot of (a) longitudinal coupons; and (b) transverse coupons.

Table 1: Longitudinal PET FRP tensile test summary

Coupon	E_1 (MPa)	E_2 (MPa)	E_3 (MPa)	ε_y (mm/mm)	F_y (MPa)	ε_h (mm/mm)	F_h (MPa)	ε_u (mm/mm)	F_u (MPa)
PET FRP- 1	5544	670	1145	0.0075	32.5	0.0326	50.1	0.0977	119.6
PET FRP-2	5540	508	1096	0.0074	33.9	0.0336	49.1	0.1033	120.2
PET FRP-3	4589	548	1133	0.0070	23.3	0.0397	45.2	0.1060	112.0
Average	5224	575	1125	0.0073	29.9	0.0353	48.1	0.1023	117.3
SD	550	84	25	0.0003	5.8	0.0038	2.6	0.0042	4.6
COV	11%	15%	2%	4%	19%	11%	5%	4%	4%

Table 2: Transverse PET FRP tensile test summary

Coupon	E_1 (MPa)	E_2 (MPa)	E_3 (MPa)	ε_y (mm/mm)	F_y (MPa)	ε_h (mm/mm)	F_h (MPa)	ε_u (mm/mm)	F_u (MPa)
PET FRP- 1	5280	374	743	0.0072	19.1	0.0249	25.7	0.0900	71.3
PET FRP-2	4606	298	627	0.0050	18.5	0.0348	29.4	0.1000	68.1
PET FRP-3	4310	280	577	0.0067	17.8	0.0347	24.5	0.0930	55.6
Average	4732	317	649	0.0063	18.5	0.0315	26.6	0.0943	65.0
SD	497	50	85	0.0012	0.6	0.0057	2.5	0.0051	8.3
COV	11%	16%	13%	18%	3%	18%	9%	5%	13%

As Figure 4 illustrates, the stress-strain profile of PET FRP could be separated into three linear curves, which is a consistent behaviour with the overall stress-strain profile of PET fibers observed in the literature (Denardin et al. 2005; Lechat et al. 2006). Hence, the three regions within the stress-strain curve—each distinguished by a different modulus—are possibly an effect of the morphological changes of PET fibers observed and reported by a previous study (Denardin et al. 2005).

4 PROPOSED STRESS-STRAIN MODEL

The stress-strain behaviour of PET FRP is comprised of three independent linear functions. The boundary and slope of each function are derived from the values presented in Tables 1 and 2. Consequently, the stress-strain relation could be described by the following piecewise function:

$$[1]\ f(\varepsilon) = \begin{cases} E_1 \cdot \varepsilon & \text{if} \quad 0 \le \varepsilon < \varepsilon_y \\ E_2 \cdot \varepsilon + c_1 & \text{if} \quad \varepsilon_y \le \varepsilon < \varepsilon_h \\ E_3 \cdot \varepsilon + c_2 & \text{if} \quad \varepsilon_h \le \varepsilon < \varepsilon_u \end{cases}$$

In which "c_1" is 25 MPa and 16 MPa for longitudinal and transverse PET FRP, respectively, whereas "c_2" is 12 MPa for the two sets of PET FRP. Figure 4 presents stress-strain models derived using the average value of each property listed in Tables 1 and 2.

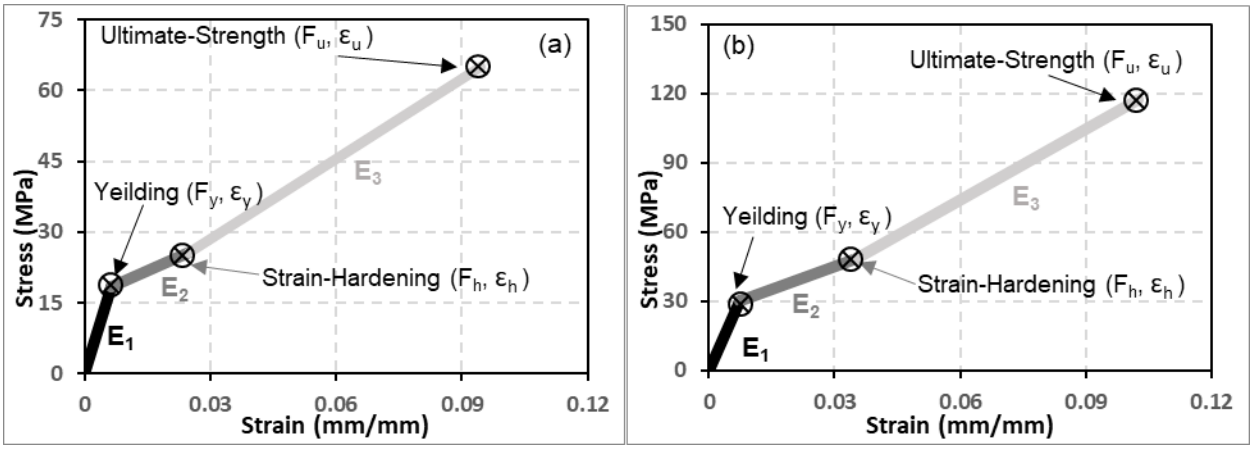

Figure 4: Stress-strain model of (a) longitudinal coupons; and (b) transverse coupons.

5 FINDINGS

In this study, six PET FRP coupons were fabricated using bio-resin. The six coupons were split into two groups: one representing coupons cut longitudinally and the other cut transversely. All coupons were tested in uniaxial tension, and the data collected was used to obtain PET FRP's mechanical properties. This includes the stress-strain relationship, yielding stress, strain at the yielding point, ultimate strength and strain, as well as moduli of elasticity before and after yielding. The stress-strain plot of PET FRP has three distinct transition regions, each with a distinct modulus and all following a linear trend. PET FRP beholds large strain capacity (four times more than GFRP's strain capacity) and relatively low strength capacity. Hence, bio-resin PET FRP cannot be used as a direct replacement for conventional FRP in applications requiring high strength component. However, it could be used as an alternative sustainable material for applications requiring a large strain capacity.

6 FUTURE RESEARCH

Future research will encompass testing additional PET FRP coupons and coupons made with epoxy to compare results provided in this study. The research will also include testing PET FRP coupons in compression to compare the tensile and compressive mechanical properties of PET FRP.

Acknowledgements

The authors would like to thank Carthage Mills for supplying the PET fabric and Pennakem for supplying the bio-resin (furfuryl alcohol and phthaloyl dichloride catalyst).

References

Applications of Geosynthetic Products | Carthage Mills, carthagemills.com/ Geosynthetic-applications.php #drainage.

ASTM. (2018). ASTM D882, Standard Test Method for Tensile Properties of Thin Plastic Sheeting. ASTM. West Conshohocken, Pennsylvania, United States.

Bachmann, J. Hidalgo, C. Bricout, S. 2017. Environmental analysis of innovative sustainable composites with potential use in aviation sector—A life cycle assessment review. Science China Technological Sciences, 1301–1317

Betts, D., Sadeghian, P., and Fam, A. 2017. Tensile Properties of Flax FRP Composites. APFIS Asia-Pacific Conference on FRP in Structures, Singapore, 1–4.

Denardin, E. L. G., Tokumoto, S. Samios, D. 2005. Stress–strain behaviour of poly(ethyleneterephthalate) (PET) during large plastic deformation by plane strain compression: the relation between stress–strain curve and thermal history, temperature and strain rate. Rheologica Acta, 142–150.

Fam, A. Eldridge, A. Misra, M. 2014. Mechanical characteristics of glass fibre reinforced polymer made of furfuryl alcohol bio-resin. *Materials and Structures*, 1195–1204.

Foruzanmehr, M. Elkoun, S. Fam, A. Robert, M. 2016. Degradation characteristics of new bio-resin based-fiber-reinforced polymers for external rehabilitation of structures. *Journal of Composite Materials*, 1227–1239.

Ghalieh, L. Awwad, E. Saad, G. Khatib, H. Mabsout, M. 2017 Concrete Columns Wrapped with Hemp Fiber Reinforced Polymer – An Experimental Study. Procedia Engineering, 440–447.

Uddin, Nasim. 2013. Developments in Fiber-Reinforced Polymer (RFP) Composites for Civil Engineering. *Woodhead Publishing Limited*,

Lechat, C. Bunsell, A. Davies, P. Piant, A. 2006 Mechanical behaviour of polyethylene terephthalate and polyethylene naphthalate fibres under cyclic loading. *Journal of Materials Science*, 1745-1756.

Lee, Luke S., and Hector Estrada. Materials for Civil Engineering: Properties and Applications in Infrastructure. McGraw-Hill, 2020.

Loong, M. L. Cree, D. 2018. Enhancement of Mechanical Properties of Bio-Resin Epoxy/Flax Fiber Composites using Acetic Anhydride. *Journal of Polymer and Environment*, 224–234.

Mamman, A. Lee, J. Kim, Y. Hwang, I. Park, N. Lee, K. Y. Chang, J. Hwang, J. (2008). Furfural: hemicellulose/xylosederived biochemical. Biofuels Bioprod Biorefin. 438– 454.

Pham, T. Hadi, M. Youssef, J. 2015 Optimized FRP Wrapping Schemes for Circular Concrete Columns. *Journal of Composites for Construction*, 1-33.